Comparison of C40/82A and P27A C40/82A Barstar Mutants Using ^{19}F NMR†

Hua Li and Carl Frieden*

Department of Biochemistry and Molecular Biophysics, Washington University School of Medicine, 660 South Euclid Avenue, St. Louis, Missouri 63110

Received December 19, 2006; Revised Manuscript Received February 13, 2007

ABSTRACT: Barstar, an inhibitor of the enzyme barnase, contains two phenylalanine residues, three tryptophan residues, and two proline residues. After incorporating either 2-^{19}F-Phe, 4-^{19}F-Phe, or 6-^{19}F-Trp, the structural, dynamic, and folding properties of two mutants (C40/82A, a double mutant, and P27A C40/82A, a triple mutant) were studied by ^{19}F NMR. Experiments were performed as a function of temperature and urea with the two mutants. We show that the consequences of the P27A mutation are extensive. The effect of the mutation is transmitted to distant residues (Phe56 and Trp53) as well as to a residue deeply buried in the hydrophobic core (Phe74). By incorporating 2-^{19}F-Phe, it is shown that Phe56 undergoes a slow ring flipping on the NMR time scale in the triple mutant that is not observed in the double mutant. On the other hand, incorporating 4-^{19}F-Phe shows that the P27A mutation has little effect along the $C^{\beta}-C^{\gamma}$ axis of Phe56. Labeling with 4-^{19}F-Phe shows, from line broadening, that Phe74 experiences more dynamic motion than does Phe56 in both the double and triple mutant. After incorporating 6-^{19}F-Trp, it is found that, in the triple mutant, Trp53 shows conformational heterogeneity at low temperature while Trp44, which is close to the P27A mutation, does not. At 20 °C, residual native-like structure was detected around Trp53 at high concentrations of denaturant. Barstar is cold denatured in the presence of urea. For the double mutant at temperatures below 15 °C, and in the presence of 2.5−3.5 M urea, the resonance for Phe74 broadens, and two peaks are observed at 5 °C indicative of an exchange process. From line-shape analysis, assuming a two-site conformational exchange, the rate constants as a function of temperature can be extracted. An Eyring plot is linear at 0 M urea but deviates from linearity below 20 °C in the presence of 2.5 or 3.5 M urea. The data as a function of urea suggest sequential events in the unfolding process.

Barstar, an intracellular inhibitor of barnase, has been extensively studied with regard to both intrinsic properties and its interaction with the enzyme barnase. X-ray (Figure 1) and NMR[1] studies of barstar show it to be composed of three parallel helices, a three-stranded β-sheet (*1*−*3*), and a barnase binding loop (Pro27−Glu32) that has been suggested to undergo conformational fluctuations (*4*). The C40/82A double mutant has been used to examine protein folding in various studies (*5*−*7*) due to the heterogeneity of the oxidation state of the cysteine and the tendency to form disulfide bonds (*3*). Barstar contains two proline residues, one of which, Pro48, is in the *cis* conformation while the other, Pro27, is *trans* in the native state. In the unfolded state, both prolines are primarily in the *trans* configuration (*6*). The P27A C40/82A triple mutant has been widely used to investigate the kinetics and structural consequences of the *trans*/*cis* isomerization of Pro48 as the protein folds (*8*−*11*). The P27A mutation may not alter barnase binding and/or inhibition as barstar is electrostatically optimized for tight barnase binding (*12*). It was found that only groups close to Pro48 in space were influenced (*9*) during the refolding of triple mutant barstar. In a study of the structural response to mutations at the barstar−barnase interface, the effects were also local (*13*). Since the side chain of Pro27 resides on a flexible binding loop distant from any side chains in the core (>7 Å), it might be expected that the P27A mutation would also have only a local effect on the

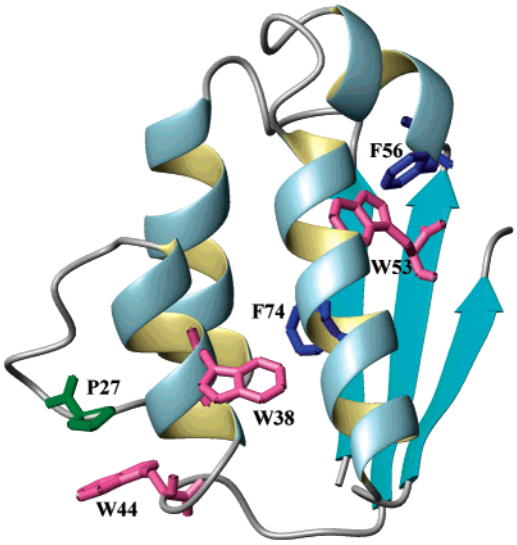

FIGURE 1: Crystal structure (PDB entry 1A19) of barstar showing the location of Pro27, the two phenylalanines, and the three tryptophans. The figure was prepared using MolMol (*50*).

† This work was supported by NIH Grant DK13332 to C.F.

* To whom correspondence should be addressed. Tel: (314) 362-3344. Fax: (314) 362-7183. E-mail: frieden@biochem.wustl.edu.

[1] Abbreviations: NMR, nuclear magnetic resonance; EDTA, ethylenediaminetetraacetic acid; TOCSY, total correlated spectroscopy; NOESY, nuclear Overhauser effect spectroscopy.

10.1021/bi6026083 CCC: $37.00
Published on Web 03/20/2007

Table 1: Distance from the Center of Pro27 to the Residues Labeled in This Study

residue	F56 (*meta*)	F74 (*meta*)	F56 (*para*)	F74 (*para*)	W38	W44	W53
d (Å)	24.0/22.0[a]	14.0/13.7[a]	22.5	12.6	14.0	3.8	18.0

[a] Distance to the two *meta* positions on the benzyl ring.

internal structural and dynamic properties in the core region. However, Pro27 has a solvent-accessible surface area of only 9 Å while that for Pro 48 is 83 Å (*8*). We show that the effects of P27A mutation are propagated to the hydrophobic core that includes Trp53, Phe56, and Phe74.

^{19}F NMR has been widely applied to biological systems to elucidate site-specific side chain information even though in rare cases fluorine substitution perturbs protein structures (*14*). Compared to ^{1}H NMR, ^{19}F NMR has a larger chemical shift dispersion, and its chemical shift is more sensitive to local environmental changes. Incorporation of fluorinated aromatic amino acids into proteins is a valuable means for delineating structural and dynamic effects as subtle as different positions of aromatic rings in interesting regions of proteins. ^{19}F NMR can also quantitatively characterize side chain dynamics such as conformational exchange (*15*). Phenylalanine and tyrosine residues are of particular interest in the structural, dynamic, and folding studies of proteins since they occur frequently in the hydrophobic cores of these molecules. For example, ring flipping has long been an interest in investigating protein dynamics and folding (*16*−*23*). However, fluctuations other than ring flipping are seldom identified and characterized (*15*, *24*).

Phenylalanine labeled with ^{19}F in the 4-position detects motions of benzyl rings other than ring flipping or motions of its microenvironments, whereas 2-^{19}F labeling can be used to study restrictions on ring flipping. In this work, the two phenylalanines (F56 and F74) were labeled with either 2-^{19}F-Phe or 4-^{19}F-Phe, and the three tryptophans (W38, W44, and W53) were labeled with 6-^{19}F-Trp for both C40/82A and P27A C40/82A mutants. Table 1 shows the distance from P27 to those labeled sites. We find that ^{19}F labeling gives structural information in both the double and triple mutant and that the P27A mutation causes significant changes to core residues distant from the mutation site in terms of internal dynamics, structural perturbation, and unfolding properties. We also show that the cold denatured state of this protein, thought to give insight into early folding events, involves side chains distant to the regions of residual structure detected by amide backbone studies (*3*).

It has long been recognized that barstar unfolds through intermediates which were detected either kinetically (*9*, *10*, *25*−*27*) or by perturbing solution conditions (*28*−*31*). Those indirectly detected intermediates were generally interpreted as either in the early or in the late stages based on fluorescence and circular dichroism studies. In this study, continuous ^{19}F chemical shift changes indeed suggest a sequential unfolding pathway.

MATERIALS AND METHODS

Chemicals. Ultrapure urea was purchased from United States Biochemical. The concentration of urea was determined by the index of refraction at 25 °C (*32*). 4-^{19}F-Phe was obtained from ACROS Organics (Morris Plains, NJ). 2-^{19}F-Phe and 6-^{19}F-Trp were obtained from Sigma-Aldrich (St. Louis, MO). All other chemicals were of reagent grade.

Incorporation of Fluoro-Labeled Amino Acids into Barstar. The production of fluoro-labeled barstar using an *Escherichia coli* bacterial expression system was essentially as described by Frieden et al. (*33*). More than 90% labeling, as indicated by mass spectroscopy (data not shown), was achieved by using the phenylalanine auxotroph DL39 and the tryptophan auxotroph W3110 containing PQE80 barstar or its mutant in defined medium.

Protein Expression and Purification. Mutants (F74L, P27A, C40/82A; W38F, P27A, C40/82A; W44F, P27A, C40/82A), which were used for NMR assignments, were made by following the protocol of the QuickChange site-directed mutagenesis kit (Invitrogen). Unlabeled barstar was expressed in LB (Luria−Bertani) medium. To incorporate fluoro amino acids into barstar, cells were grown to an A_{600} of 3 in defined medium, then harvested, and resuspended in a fresh defined medium containing 0.2 mM of the desired specifically fluoro-labeled amino acid. After 30 min, protein production was induced with 1 mM isopropyl β-D-thiogalactoside (IPTG) for 3 h for ^{19}F-Phe labeling and 6 h for 6-^{19}F-Trp labeling. Protein purification was essentially the same as described previously (*2*) except that an ion-exchange column was used before gel filtration. P27A C40/82A barstar and its mutants were recovered from inclusion bodies (*10*). The production of the labeled proteins is comparable to the unlabeled protein with a yield of ∼6−10 mg/L of medium.

Sample Preparation. For NMR spectra as a function of urea, samples were made by dilution of a stock protein solution into the NMR buffer (containing 20 mM sodium phosphate and 0.25 mM EDTA, pH 6.7) plus varying amounts of a 9.2 M urea stock solution dissolved in the NMR buffer to give a final concentration of 100 μM protein and different urea concentrations. The sample for fluorescence studies was made the same way with a final protein concentration of 1.5 μM. All of the samples were made by adding the protein stock to the premixed solution of the other components.

Fluorescence Spectroscopy. Steady-state fluorescence experiments as a function of urea were performed at 20 °C using a PTI Alphascan fluorometer (Photon Technology International, South Brunswick, NJ). The excitation wavelength used was 290 nm, and the emission spectra were recorded between 300 and 400 nm. Equilibrium data were fit to a two-state model as described by Ropson et al. (*34*) using the equation of Santoro and Bolen (*35*).

^{19}F NMR Spectroscopy. ^{19}F NMR spectra were acquired on a Varian Unity-Plus 500 MHz spectrometer operating at 470.3 MHz with a Varian Cryo-Q dedicated to a 5 mm ^{19}F probe without ^{1}H decoupling. The ^{19}F probe was cooled and kept at 20 K with the Varian Cryo-Q open cycle cryogenic system. All 1D spectra were recorded with 128 scans and 3 s recycle delay and processed by NMRPipe (*36*) with 12 Hz exponential line broadening unless otherwise indicated. All samples contained 8% (v/v) D_2O. There was no correction to the pH value due to D_2O.

Line-Shape Analysis. A series of 1D ^{19}F NMR spectra were recorded for the double mutant at 0, 2.5, and 3.5 M urea with temperature from 5 °C (or 2 °C) to 35 °C. At each temperature, the sample was allowed to equilibrate for at least 10 min. Simulated spectra at different temperatures were

calculated using line-shape analysis software [Mexico program (*37*)] assuming two-site equally populated exchange. The line width for the two sites was assumed to be the same. The Varian experimental data sets were converted to an ASCII file with the *x*-axis in frequency (hertz) in order to be compatible with the Mexico program. In the simulation, the rate and one of the frequencies were allowed to be varied. To extract thermodynamic parameters for the exchange, Eyring plots [ln(k/T) vs $1/T$] were obtained by fitting experimental rate constants to the Eyring equation (*38*), i.e.

$$\ln\left(\frac{k}{T}\right) = -\left(\frac{\Delta H^{\ddagger}}{R}\right)\left(\frac{1}{T}\right) + \frac{\Delta S^{\ddagger}}{R} + \ln\left(\frac{\kappa}{h}\right)$$

where R, κ, and h are the universal gas contant, Boltzmann's constant, and Planck's constant, respectively. $\Delta H^{\ddagger}$ and $\Delta S^{\ddagger}$ were assumed to be independent of T for the temperature range studied [2 °C (or 5 °C) to 35 °C].

^{1}H NMR Spectroscopy. Homonuclear NOESY and TOCSY experiments were carried out on a Varian 600 MHz spectrometer at 25 °C with the double mutant at a protein concentration of ~1.2 mM. The spectra were recorded with 2048 complex data points in t_2 and 512 increments in t_1 with a spectrum width of 7200 Hz in both dimensions. Each increment takes 32 scans. Mixing times were 150 and 50 ms for NOESY and TOCSY, respectively. The data were processed by NMRPipe (*36*).

Sedimentation Equilibrium. Sedimentation equilibrium ultracentrifugation was performed at 20 °C for both mutants with four samples (unlabeled and 2-^{19}F-Phe, 4-^{19}F-Phe, and 6-^{19}F-Trp labeled) using an Optima XL-A analytical ultracentrifuge (Beckman Instruments, Fullerton, CA). Three rotor speeds (32K, 39.2K, and 48K) were used with three concentrations (50, 100, and 200 μM), monitoring absorbance at 295, 300, and 305 nm. The data were analyzed by WinNONLIN and WinREEDIT (ftp://spin.mcb.uconn.edu).

RESULTS

Sedimentation Equilibrium Studies. The sedimentation equilibrium studies indicated that all proteins used in this study are monomeric at protein concentrations below 200 μM, the highest concentration used in the NMR experiments (data not shown). Thus, none of the observed effects described below are a consequence of dimer formation.

Assignment of ^{19}F Resonances. The NMR assignments are shown in Figure 2 with details included in Supporting Information (Figure S1). Peaks marked with an asterisk in Figure 2 are reference peaks. Small amounts of denatured peaks (labeled U) were observed for all of the triple mutants even under native conditions. The percentage of unfolded-like species is 7.7%, 5.2%, and 10% for protein labeled with 2-^{19}F-Phe, 4-^{19}F-Phe, and 6-^{19}F-Trp, respectively. The appearance of unfolded-like species is probably a consequence of the slightly lower stability of triple mutant and is consistent with results reported previously (*10*) and not due to fluorine labeling.

Effect of ^{19}F-Labeling on Structure. Fluorine labeling did not detectably disrupt the native structure in either the double or triple mutant, with 2-^{19}F-Phe and 6-^{19}F-Trp labeling only slightly less stable than the unlabeled protein (Figure 3). The 4-^{19}F-Phe-labeled protein is at least as stable as the unlabeled

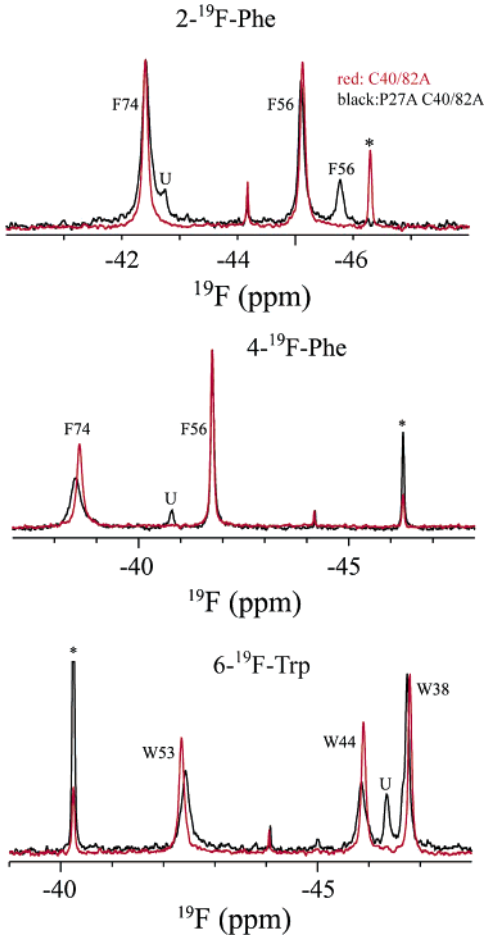

FIGURE 2: NMR assignments of 2-^{19}F-Phe-, 4-^{19}F-Phe-, and 6-^{19}F-Trp-labeled barstar. Red and black spectra represent the double (C40/82A) and triple (P27A C40/82A) mutants, respectively. The spectra were acquired at 20 °C and processed as described in the text. The sharp peak around −44.1 ppm is from a transmitter offset frequency (tof) glitch. The peaks labeled U are unfolded resonances. The peaks marked with an asterisk (*) are references, which are 6-^{19}F-Trp (the actual chemical shift is −46.293 ppm relative to TFA) for 2-^{19}F-Phe and 4-^{19}F-Phe assignment and 4-^{19}F-Phe (the actual chemical shift is −40.244 ppm relative to TFA) for 6-^{19}F-Trp assignment. In the lowest black spectrum, the shoulder peak around −46.6 ppm is also from the unfolded species.

protein (Figure 3). To determine the effect of fluorine labeling on protein structures, we performed proton TOCSY and NOESY experiments for the double mutant for the four different samples (unlabeled and 2-^{19}F-Phe, 4-^{19}F-Phe, and 6-^{19}F-Trp labeled,) and the spectra are superimposable. The only significant chemical shift deviations are from the protons in the same labeled aromatic ring as expected (data not shown).

Comparison of the Two Mutants at 20 °C after Labeling with 2-^{19}F-Phe. Phe56 is 24 Å from Pro27 while Phe74 is 14 Å away and deeply buried in the hydrophobic core. In the triple mutant, Phe74 exhibits one broadened peak while Phe56 shows two peaks with different intensities (Figure 2, top, black line), indicating that Phe74 has more rotational freedom along the $C^{\beta}-C^{\gamma}$ axis of the benzyl ring while the rotation of Phe56 is restricted. The two conformations of Phe56 in the triple mutant are in slow exchange on the NMR time scale as no exchange cross-peaks were observed in phase-sensitive ^{19}F−^{19}F NOESY by increasing temperature up to 35 °C or by urea denaturation (data not shown).

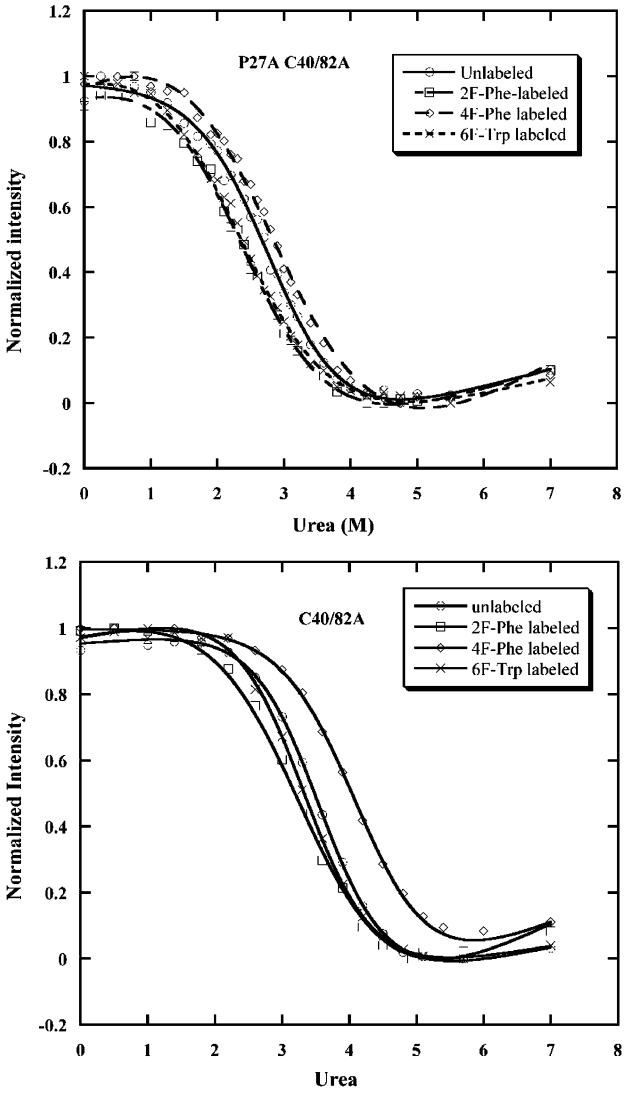

FIGURE 3: Equilibrium unfolding of unlabeled and 2-^{19}F-Phe-, 4-^{19}F-Phe-, and 6-^{19}F-Trp-labeled double and triple mutants at 20 °C. Unfolding was followed by monitoring fluorescence at 327 nm with excitation at 290 nm. Sample conditions are described in the text. Data were fit using the equation of Santoro and Bolen (*35*).

Although different temperature coefficients ($\Delta\delta/\Delta T$) (Figure 4A) for the major and minor conformations indicate magnetically different environmental changes, their line width changes with temperature are almost identical (Figure 4B), suggesting similar dynamic properties for the two conformations. In the triple mutant, the line width of Phe56 decreases with increasing temperature at temperatures below 20 °C, indicating that the side chain of Phe56 is dominated by motions in a fast time regime. At temperatures above 20 °C, however, fluctuations of Phe56 in the slow exchange regime start to dominate, which causes the line width to increase slightly with increasing temperature. It should be noted that the minor conformation shifts toward the more favorable major conformation with increasing temperature (Figure 4B, inset) possibly because high temperatures lower the rotational barrier along the $C^{\beta}-C^{\gamma}$ axis of the phenyl group.

The double mutant shows two peaks of almost the same intensity for the two phenylalanines (Figure 2, top). The temperature coefficient of 2-^{19}F-Phe56 in the double mutant

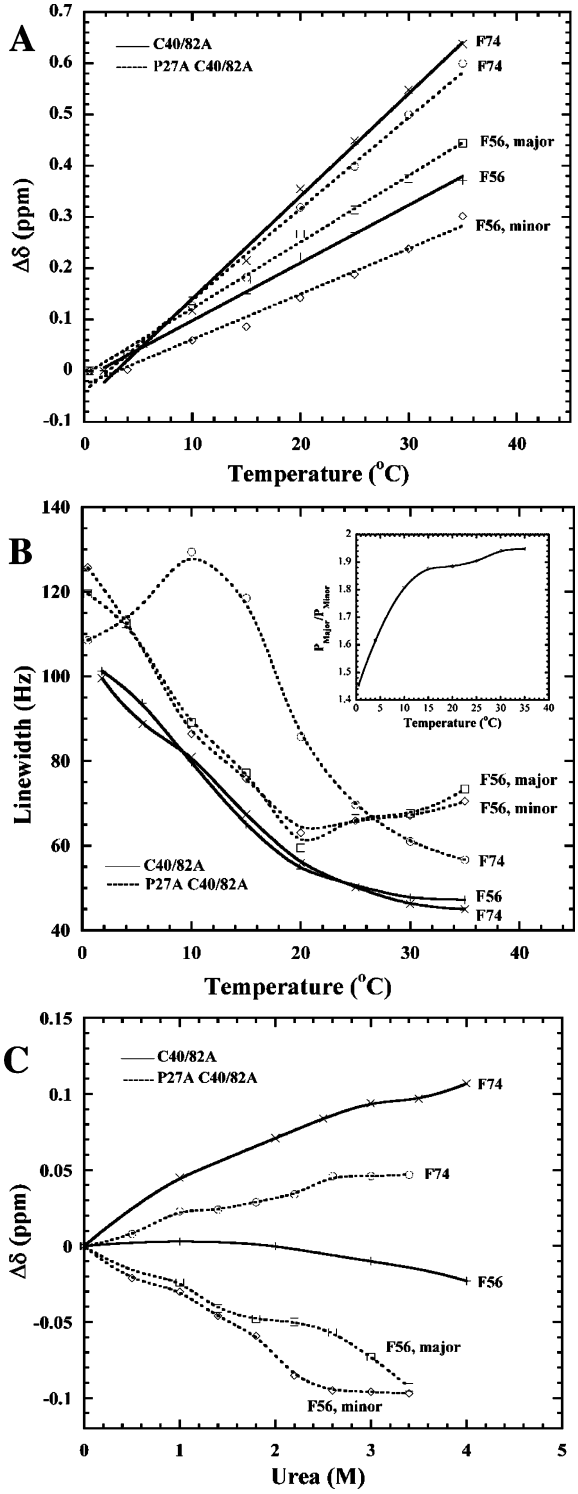

FIGURE 4: ^{19}F NMR results for 2-^{19}F-Phe-labeled double and triple mutants showing the temperature coefficient (A), line width change vs temperature (B), and chemical shift changes vs urea concentrations at 20 °C (C). The inset in (B) shows the population ratio change with temperature for the two conformations of Phe56 in the triple mutant. $\Delta\delta$ stands for chemical shift changes.

is similar to that in the triple mutant while the line width is slightly less (5−10 Hz on average). In the double mutant, the line width of Phe56 decreases with increasing temperature, indicating fluctuations in the fast time regime.

Phe74 shows a single peak in both mutants each with similar temperature coefficients. In the triple mutant, however, Phe74 shows dramatic line broadening compared to

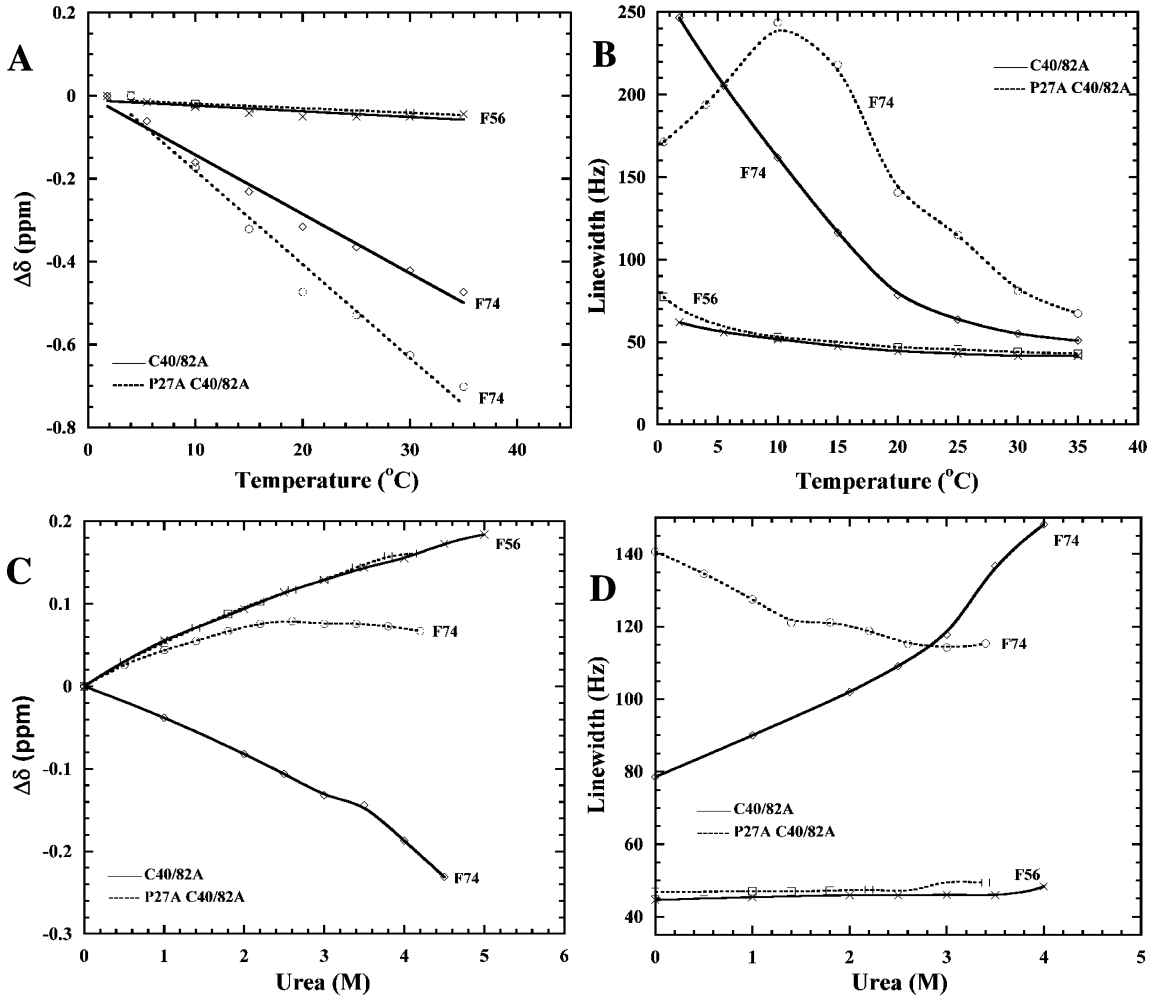

FIGURE 5: ^{19}F NMR results for 4-^{19}F-Phe-labeled C40/82A and P27/40/82A barstar showing the temperature coefficient (A), line width changes vs temperature (B), chemical shift changes vs urea concentrations at 20 °C (C), and line width changes vs urea concentration at 20 °C (D).

double mutant (Figure 4B), indicating that Phe74 is sensitive to the P27A mutation.

Upon urea denaturation at 20 °C, the overall chemical shift changes are marginal for both mutants (Figure 4C) with each residue changing in the same direction (but not to the same extent). Their line widths do not change with urea (data not shown).

Comparison of the Two Mutants at 20 °C after Labeling with 4-^{19}F-Phe. After labeling with 4-^{19}F-Phe, Phe56 and Phe74 show single peaks for both mutants (Figure 2, middle). The temperature and urea dependence is the same for Phe56 in both the double and triple mutant, while Phe74 shows a dramatically different dependence (Figure 5), suggesting that the P27A mutation has a larger effect on Phe74 than on Phe56. Phe74 shows a larger negative temperature coefficient and a broader line width change in the triple mutant than in the double mutant (Figure 5A,B), suggesting that Phe74 in the triple mutant is less restricted by its surroundings and senses more motional freedom perhaps because of inefficient packing due to P27A mutation. The different chemical shift and line width changes with urea of Phe74 in the triple mutant also demonstrate that the structure and dynamics around Phe74 are quite different in those two mutants (Figure 5C,D).

The line width of Phe74 in the triple mutant decreases with increasing urea, suggesting additional fast motions upon urea denaturation. In the double mutant, however, the line width of Phe74 increases with increasing urea, indicating additional slow motions during urea denaturation. In the course of urea denaturation of the double mutant, the line width of denatured peak remains unchanged, and there is no overall intensity loss (data not shown). Therefore, the line broadening of Phe74 in the double mutant is less likely to be caused by exchange between the folded and unfolded form but rather due to exhibiting multiple conformers that are in intermediate to slow exchange. To test this hypothesis, temperature studies were obtained for protein solutions containing 0, 2.5, and 3.5 M urea (Figure 6). The peak of Phe74 is dramatically broadened with decreasing temperature, and at 5 °C, two peaks of almost the same intensity are observed at 2.5 M urea (Figure 6B). Below 20 °C, cold denaturation occurs at 2.5 and 3.5 M urea as shown by Wong (*39*).

Cold Denaturation and Line-Shape Analysis for 4-^{19}F-Phe74 in the Double Mutant. It has been shown that, in the presence of 3 M urea, the double mutant is completely denatured at 5 °C (*39*) using ^{1}H, ^{15}N, and ^{13}C NMR. In our study, we found that the double mutant is not completely denatured even at 3.5 M urea at 5 °C (Figure 6C). Moreover, we observed conformational exchange of Phe74 in the intermediate time scale in 3.5 M urea (Figure 6C). The temperature-dependent exchange rate was determined by

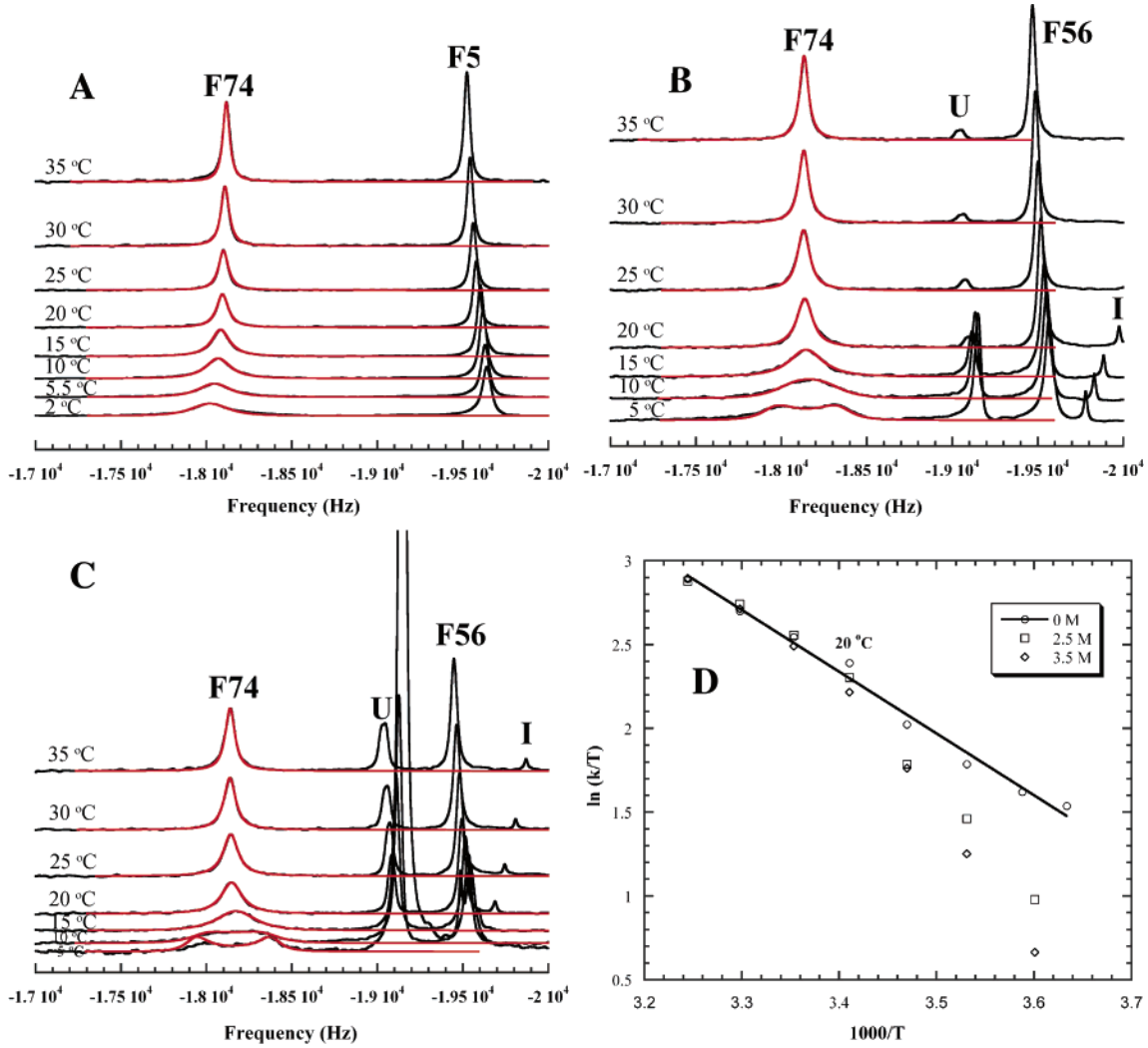

FIGURE 6: Line-shape analysis for 4-^{19}F-Phe-labeled double mutant barstar containing 0 M (A), 2.5 M (B), and 3.5 M (C) urea at different temperatures. Black and red spectra represent experimental data and simulation results, respectively. For each temperature, the simulated region (red) is from −20000 to −17300 Hz (−42.52 to −36.78 ppm) assuming two-site equally populated exchange. The peak labeled U is unfolded, and the one labeled I is a tof glitch. (D) Eyring plot based on exchange rates extracted from simulations.

means of line-shape analysis. On the basis of the observation of two peaks of equal intensity at 2.5 M urea, we assume two-site equally populated exchange. This model was adequate to fit all of the data sets except at high urea concentration and low temperatures. Experimental spectra, simulations, and exchange rate constant data in the form of an Eyring plot are shown in Figure 6. The Eyring plot shows a linear correlation for two conformational exchanges and yields activation parameters $\Delta H^{\ddagger} = 30.6$ kJ·mol^{-1} and $\Delta S^{\ddagger} = -74$ J·mol^{-1}·K^{-1} at 0 M urea. The plot deviates from linearity at 2.5 and 3.5 M urea at 20 °C, below which cold denaturation occurs (Figure 6D). The deviation may be related to cold denaturation or a small amount of intermediates that becomes more important at the lower temperatures.

Comparison of the Two Mutants at 20 °C after Labeling with 6-^{19}F-Trp. In the crystal structure, Trp44 is close to the P27A mutation site while Trp38 and Trp53 are distant (Table 1). Further, Trp38 is solvent exposed while Trp53 is buried.

The temperature coefficients ($\Delta\delta/\Delta T$) are very similar in the double and triple mutants for both Trp53 and Trp38 while Trp44 shows a temperature coefficient of different sign (Figure 7A). The line width change of Trp38 is negligible (Figure 7B) probably because it is solvent exposed. But the line widths of Trp44 and Trp53 in the triple mutant are broader than those of their corresponding residues in the double mutant (Figure 2, bottom, and Figure 7B), which is consistent with results revealed by 2-^{19}F-Phe and 4-^{19}F-Phe labeling. Collectively, the data demonstrate that the triple mutant has greater motional freedom.

For the double mutant, the line width of all of the tryptophans decreases with increasing temperature, suggesting motions in a fast exchange regime. But for the triple mutant, the unusual behavior of the line width of Trp53 and Trp44 at low temperatures (Figure 7B) indicates dynamics in a slow time regime. This is very obvious at 0.5 °C as the broad peak of Trp53 that is present at higher temperatures splits into at least three peaks (Figure 8A).

On denaturation as a function of urea at 20 °C, Trp38 shows similar chemical shift changes in the two proteins as does Trp53 at urea concentrations below 2.6 M (Figure 7C). At urea concentrations above 2.6 M, their chemical shift changes start to deviate, which is caused by the splitting of the Trp53 resonance in the triple mutant (Figure 8B). Trp44 shows quite different chemical shift changes with urea in the two mutants (Figure 7C), similar to its temperature

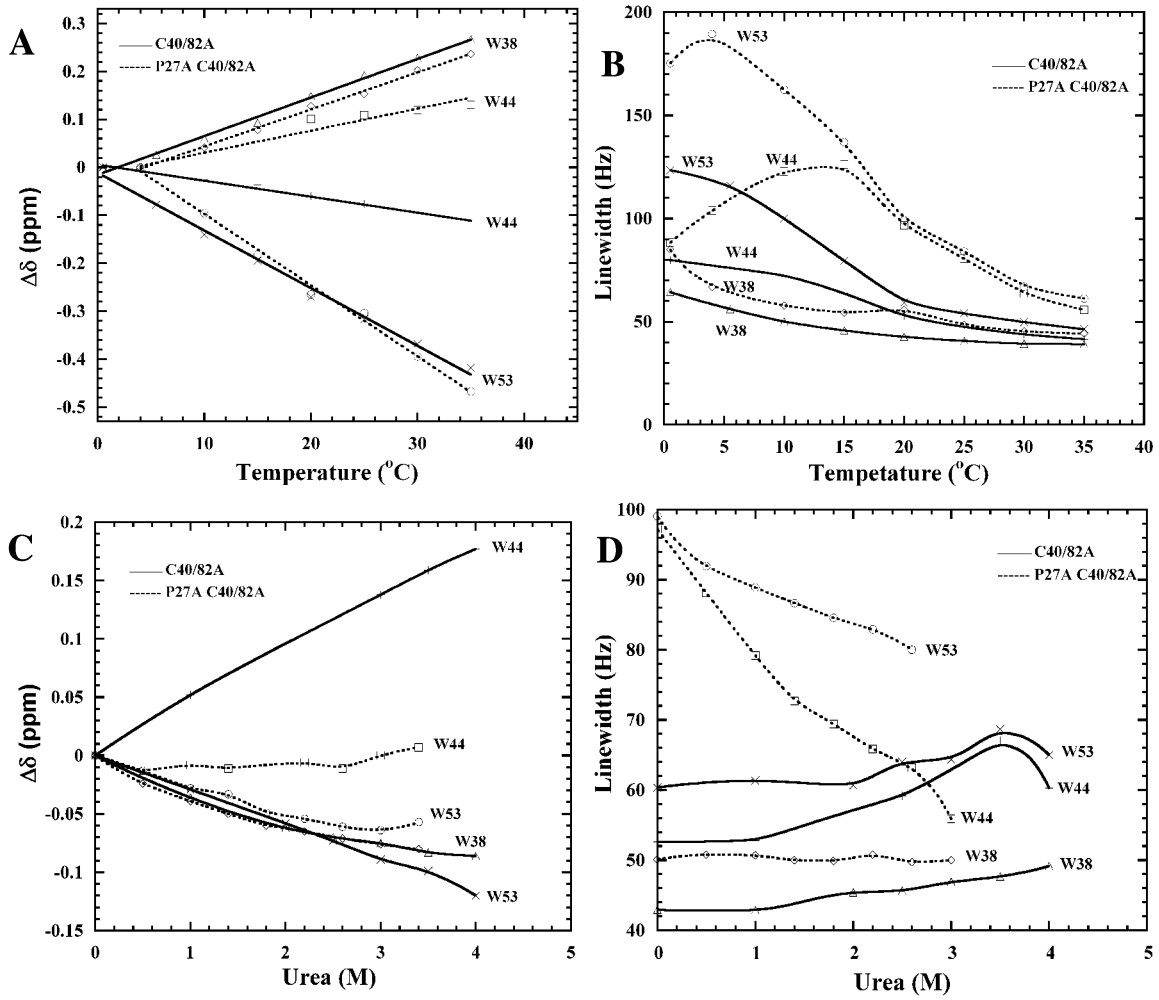

FIGURE 7: ^{19}F NMR results for 6-^{19}F-Trp-labeled double and triple mutants showing the temperature coefficient (A), line width changes vs temperature (B), chemical shift changes vs urea concentrations at 20 °C (C), and line width changes vs urea concentration at 20 °C (D). Due to splitting, the line width of Trp53 is only plotted to 2.6 M urea. In (B), the line width of the major conformation of Trp53 in the triple mutant was used at 0.5 °C.

dependence, probably because Trp44 is very close to the mutation site (~3.8 Å). There is no significant line width change with urea concentration for all of the tryptophan residues in the double mutant as with Trp38 in the triple mutant (Figure 7D). In the triple mutant, however, Trp44 shows a decreased line width with increasing urea concentration as is true for Trp53 up to 2.6 M urea. The line width of Trp53 in the triple mutant broadened at 3.0 M urea due to a growing shoulder peak which appears at 1.8 M urea (Figure 8B), which increases relative to the left side major peak. Those two peaks persist even at high urea concentrations (0.5%−1% total intensity, Figure 8B) suggesting residual native-like clusters in the unfolded state. The P27A mutation causes structural and dynamic changes not only to the local residue (Trp44) but also to the core residue Trp53, which is ~18 Å away from the mutation site, while the influence at Trp38 (~14 Å away), which is exposed to solvent, is relatively small.

DISCUSSION

The double (C40/82A) and triple (P27A C40/82A) mutants of barstar have been extensively used in studies of the structure, dynamics, and folding. Both proteins eliminate the possibility of forming intermolecular disulfide bonds while the triple mutant eliminates any complications from isomerization of Pro27 while allowing exploration of the role of the *cis*/*trans* isomerization of the remaining proline at position 48, which is *cis* in the native structure. The presumption has been that the additional P27A mutation would not affect the properties of the protein. We show here that this presumption is not correct. Additionally, we show that the use of fluorine-labeled amino acids provides detailed information about side chain behavior which may not be obvious from other NMR techniques.

Table 1 shows the distance of Pro27 to the residues that have been labeled with fluorine. Only the fluorine group of 6-^{19}F-Trp44 is close to the P27A mutation site while others are distant (>12 Å). Yet the effect of the P27A mutation is profound as measured by the chemical shifts and line widths of the labeled amino acid residues. The behavior of each of the labeled residues is discussed below.

2- and 4-^{19}F-Phe56. The asymmetry of ^{19}F-Phe substituted in the 2 (*meta*) position provides a way to examine the side chain environment along the edge of the phenylalanine and any restriction of ring flipping. Figure 2, top, shows two peaks for the triple mutant but not the double mutant, suggesting that ring flipping is slow on the NMR time scale at 20 °C. Thus this residue exists in two conformations with

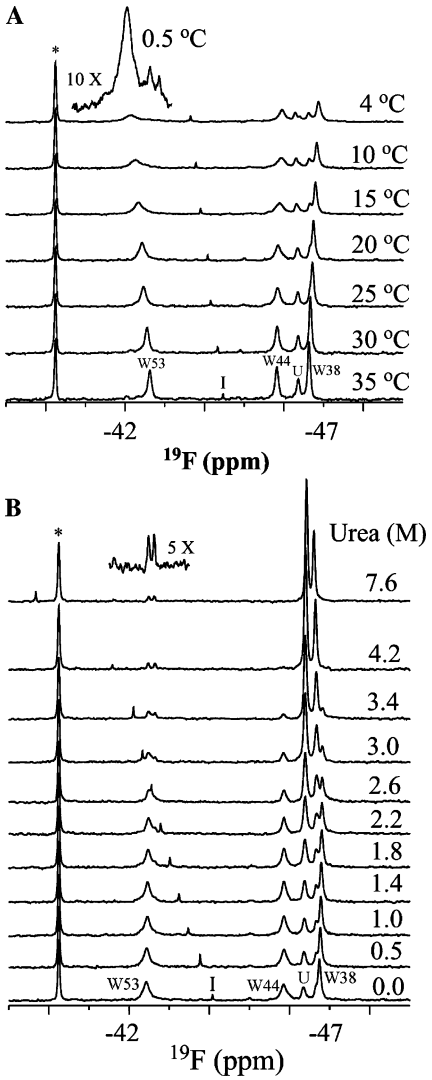

FIGURE 8: ^{19}F NMR spectra for the 6-^{19}F-Trp-labeled triple mutant as a function of temperature (A) and urea at 20 °C (B). The peak labeled U and the shoulder of W38 are from unfolded-like species. The peak labeled I is a transmitter offset frequency glitch, and the peaks labeled with an asterisk are 4-^{19}F-Phe used as reference. The labels 10× and 5× stand for 10 and 5 times scaled to the spectrum immediately below it.

unequal populations with a high barrier to their interconversion. The resonance of 2-^{19}F-Phe56 in the double mutant is superimposable with the major conformation in the triple mutant (Figure 2, top), suggesting that the rotation of 2-^{19}F-Phe56 in the double mutant is restricted on the NMR time scale as well. It had previously been suggested that the aromatic rings of both Phe56 and Phe74 flip rapidly on the chemical shift time scale since the 2- and the 3-protons of Phe56 and Phe74 of wild-type bastar (*2*) and the C40/82A mutant (*3*) have degenerate ^{1}H chemical shifts. However, our ^{19}F NMR study indicates that the rotational motions of 2-^{19}F-Phe56 are slow on the NMR time scale with 2-^{19}F-Phe56 adopting two conformations in the triple mutant, probably due to loose packing, and one conformation in double mutant.

On inspection of the X-ray crystallographic structure of barstar (PDB entry 1A19) (*1*), Phe56 and Trp53 adopt an edge to face conformation with the 2-proton of Phe56 on top of the indole ring of Trp53 (Figure 1). With 2-^{19}F-Phe labeling, electrostatic interactions between the highly electronegative fluorine nucleus and relatively negative indole ring may determine the conformational orientation with 2-^{19}F pointed away from the indole ring. Depending on the tightness of protein packing and subtle environmental changes, however, the 2-position of Phe56 may adopt a conformation other than pointing away from the indole ring. For this reason, the 2-position of Phe56 may adopt two conformations in the triple mutant. The major peak at −45 ppm, which reflects less shielding effect from the indole ring, could be assigned to the conformation with the 2-position away from the indole ring while the minor peak at −45.7 ppm, which reflects a larger shielding effect, could be assigned to the other conformation.

The restricted rotation of Phe56 in both mutants is probably not influenced by fluorine labeling but is an inherent property of unlabeled Phe56. This conclusion is based on the following reasons. First, chemical shift degeneracy (*3*) does not necessarily lead to the conclusion that exchange among different conformations is fast. Rather, it only suggests that different conformations sense the same net magnetic environment. Second, based on the analysis of the crystal structure, the partially positively charged hydrogen on the edge of the Phe56 interacts favorably with the negatively charged indole face of Trp53. Rotation of Phe56 to allow the other edge to interact with indole face would have to overcome an energetically unfavorable state with Phe56 transiently stacking on the face of Trp53. Third, ring flipping is a large amplitude motion involving major rearrangements of its surroundings. A fluorescence study of the Trp38/44Phe mutant suggests that the environment of Trp53 is very rigid (*40*), and our NMR studies confirm this finding. Finally, the result revealed by ^{19}F NMR is consistent with molecular dynamics (MD) simulations that only ring flipping of F74 is energetically possible (*41*).

Although the P27A mutation causes a dramatic influence along the edge of Phe56, it has little effect along the $C^{\beta}-C^{\gamma}$ axis of Phe56. The small temperature coefficient of 4-^{19}F-Phe56 is an indication that its 4-position is strongly associated with its surroundings and that its movement other than rotation is highly restricted. This also accounts for the observation that the line width of Phe56 is almost unchanged with temperature and urea denaturation (Figure 5). On the basis of the X-ray crystallographic structure of barstar, the restriction may be imposed by the methyl group of Ala67 and the backbone of Ala67 and Glu68 since they are less than 4.5 Å from the 4-position of Phe56 and they themselves are highly restricted with order parameters larger than 0.85 (*41*). Since the environment of Trp53 is very rigid (*40*) and the rotational motion of Phe56 is restricted, we speculate that those restrictions could influence motion other than flipping of Phe56 as Phe56 and Trp53 adopt a face-to-edge conformation with the distance between the edge of Phe56 and the center of Trp53 less than 4.5 Å.

2- and 4-^{19}F-Phe74. Unlike the response of Phe56 to the P27A mutation, Phe74 sensed the P27A mutation along both its edge and its axis. In general, Phe74 is structurally and dynamically more perturbed in the triple mutant, and there is a more profound effect toward cold denaturation than Phe56 (see below). The influence along the $C^{\beta}-C^{\gamma}$ axis is more apparent than that on the edge. As the 4-position of benzyl ring would not sense any environment change through flipping along the $C^{\beta}-C^{\gamma}$ axis, its chemical shift and line

width changes in response to temperature may reflect two possibilities: either an indication that the spatial orientation of the rotation axis of 4-^{19}F-Phe74 varies somewhat during the rotational movements or that there are fluctuations in the environment. The hydrophobic core in barstar is composed of 10 leucines, 3 valines, 4 isoleucines, Trp53, Phe56, Phe74, Ala3, Ala67, and Ala77 (*2*). Among the residues whose side chains are <5 Å to the 4-proton of Phe74 are Leu20, Leu24, Leu37, Leu41, Leu51, and Val70. Their methyl groups exhibit a wide range of dynamic behavior according to molecular dynamics simulations (*41*). The mobility of the side chains around Phe74 could be related to the temperature and urea denaturation behavior of Phe74 regarding both edge and axis orientation. Thus, different experimental observations of fluctuations provide information about the dynamics of the hydrophobic cluster in the protein interior. Moreover, the fluctuations manifested by the side chain of Phe74 are not just localized but susceptible to long-range effects from distant mutations (12.6 Å).

It is interesting to note that for both the 2-^{19}F- and 4-^{19}F-Phe-labeled triple mutant (but not the double mutant), there is a major dynamic transition at 10 °C for Phe74 (Figures 4B and 5B); i.e., below 10 °C exchange in a slow regime dominates while exchange in the fast range dominates above 10 °C. This observation may explain the phenomena described previously (*10*) that the triple mutant showed smaller amplitude in the near-UV CD signal at 10 °C and there were small differences in the fine structure relative to the double mutant. Our work indeed shows that the P27A mutation changed the dynamic behavior of the most buried side chain (Phe74) even though the 4-position of Phe74 is 12.6 Å away from the ring center of Pro27.

Thermodynamics of Phe74 in the C40/82A Double Mutant. The conformational exchange for Phe74 shows a lower activation barrier than the ring flipping in other systems (*17*−*21*) and a very small $\Delta S^{\ddagger}$ value (−74 J·mol^{-1}·K^{-1} in 0 M urea). Due to the small temperature range studied, the activation entropy ($\Delta S^{\ddagger}$) derived from Erying plots could be associated with considerable uncertainty; nevertheless, the sign and magnitude of $\Delta S^{\ddagger}$ at 0 M urea suggest that, in the transition state of the conformational exchange, Phe74 is more ordered as a consequence of interaction with other residues. It may also indicate a transition state with solvent reorganization, i.e., coordination of additional solvent. The transition state of ring flipping, however, is completely different. Ring flipping is related to the larger amplitude of breathing through displacing neighboring groups to release the steric hindrance opposing the rotational motions. In other words, the transition state for ring flipping is less ordered than the ground state. This aspect of ring flipping could explain the large positive value reported for most ring flipping processes. However, some ring flipping reactions do have negative $\Delta S^{\ddagger}$. The reported smallest value of $\Delta S^{\ddagger}$ for ring flipping is -16.7 ± 4.2 J·mol^{-1}·K^{-1} in the study of BPTI (*21*), while other well-characterized ring flippings of BPTI, cytochrome *c*, and iso-cytochrome *c* exhibit $\Delta S^{\ddagger}$ values between 96 and 301 J·mol^{-1}·K^{-1} (*21*).

In the triple mutant, Phe74 also shows motions other than ring flipping in the intermediate to slow time regime (Figure 5B). Yet no line-shape analysis was performed on Phe74 in the triple mutant due to lack of information regarding the number of exchange species and their population ratios.

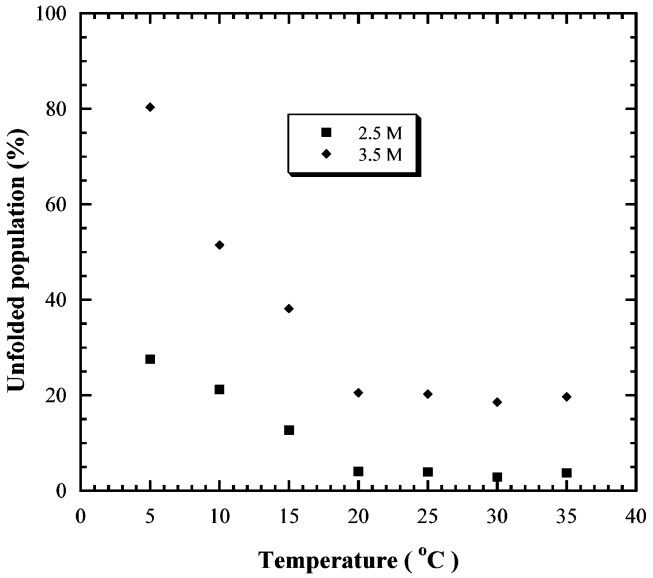

FIGURE 9: Normalized unfolded population in the cold denaturation of the 4-^{19}F-Phe-labeled double mutant in 2.5 and 3.5 M urea as a function of temperature.

Cold Denaturation of the Double Mutant. It has been reported that, in the presence of 3 M urea, the double mutant can be completely denatured at 5 °C (*39*). Studies based on NOEs, chemical shift deviations, and $^{3}J_{HN-H\alpha}$ coupling constants have suggested residual structure in this cold denatured barstar in regions corresponding to the first and second helices and near the end of the second β-strand, whereas the C-terminal region (Asn65 to Ser89) is in a random coil conformation (*39*). Our ^{19}F NMR results are not totally consistent with the above observations. First, even taking into account that 4-^{19}F-Phe labeling makes the protein slightly more stable, the protein is not completely denatured at 5 °C in the presence of 3.5 M urea (Figures 6C and 9), suggesting that side chain interactions are sometimes more resistant to denaturation than interactions involving the backbone, an observation also made in the study of the urea denaturation of the intestinal fatty acid binding protein (*42*, *43*). Second, in addition to the presence of the native-like Phe56 resonance at 5 °C, the residual structure persists around Phe74, which undergoes conformational exchange on an intermediate to slow time scale (microsecond to millisecond). As their chemical shifts (in 3.5 M urea at 5 °C) are similar to those under native conditions, the residual structures formed around the side chains of Phe56 and Phe74 are native-like, which is not consistent with the conclusion drawn from previous studies (*39*). The cold denaturation results (*39*) also show a discrepancy with the urea denaturation of barstar when the propensities of the secondary structure of the residual structure during unfolding (*44*) are investigated. Although the discrepancy may be due to different denaturation methods, neither of the two studies consider that whatever the propensity of secondary structure is, it is probably initiated by the more stable side chain interactions.

It might be noted that urea frequently induces cold denaturation (*45*). Studies of the side chain residual structure using ^{19}F-labeled amino acids may be complementary to

NMR studies at very cold temperatures in reverse micelles as has been studied by Wand and co-workers (*46*, *47*).

Tryptophans. The P27A mutation has little effect on Trp38, which is exposed to solvent and distant (14 Å) from the mutation site. Structural and dynamic changes, however, are observed for both Trp44 and Trp53, even though the latter is also distant (18 Å) from the point of the mutation. In addition, the P27A mutation also causes changes in folding properties as the residual structure around Trp53 was observed in the urea-denatured triple mutant (Figure 8B).

It has been shown by fluorescence that the hydrophobic burial of aromatic side chains is slightly increased when studying cold and heat renaturation of the triple mutant (*10*). In Figure 8B, we observed some residual structures at high urea concentration (7.6 M) in the triple mutant, perhaps complement to the aforementioned fluorescence results (*10*) that a small amount of native-like Trp53 accounts for the burial. The two conformations of Trp53 (Figure 8B) may indicate increased dynamics or dynamics of its environment of a native-like cluster on a slower NMR time scale at high urea concentrations.

Urea Unfolding of Barstar Is Sequential. A full understanding of folding/unfolding requires examination of all interactions involved such as backbone conformation, hydrogen bonding, electrostatic and hydrophobic forces. NMR is probably one of few means to be approaching this goal. Recent work includes the study of BBL (*48*) and our previous work of IFABP using ^{15}N and ^{19}F NMR (*42*, *43*). Those studies suggest an unsynchronized unfolding pathway. Barstar, as suggested by the continuous chemical shift changes with urea (Figures 4, 5, and 7), provides another example that structural changes occur before complete unfolding, consistent with the study of Lakshmikanth et al. (*49*) using the time-resolved fluorescence resonance energy transfer method. The results also demonstrate noncoincident unfolding transitions in different parts of the protein as suggested by the different pattern of chemical shift changes for different resonances.

In conclusion, ^{19}F NMR provides a useful means to study protein conformational changes. Important information, which may not be accessible by other techniques, can be extracted from apparently simple data sets such as chemical shift and line width changes. This kind of study is especially useful in the folding/unfolding studies as protein structure changes with time or denaturant, which other NMR techniques may fail to follow due to chemical shift overlap. Most importantly, it also provides site-specific side chain information which is rarely accessible by other methods. In this study, ^{19}F NMR reveals that the effect of the P27A mutation propagates structural, motional, and folding changes to distant core residues. This study may suggest a general phenomenon in that the interior of a protein forms a dynamic network. Residues in the protein core appear to sense changes in the dynamic network from distant regions of the protein, such as Phe56 senses the mutation of P27A from the edge (2-substitution) not the axis (4-substitution). This could be very important in folding of small proteins if core residues form native contacts first resulting in stabilization of those residues which are distant from the core.

ACKNOWLEDGMENT

The authors thank Dr. Linda Kurz for helpful suggestions, Dr. Anita Niedziela-Majka for excellent help with the analytical ultracentrifugation experiments, Mr. Bob Horton for technical assistance, and Dr. Ralph Golbik for providing the P27A C40/82A plasmid.

SUPPORTING INFORMATION AVAILABLE

One figure containing ^{19}F NMR assignments. This material is available free of charge via the Internet at http://pubs.acs.org.

REFERENCES

1. Ratnaparkhi, G. S., Ramachandran, S., Udgaonkar, J. B., and Varadarajan, R. (1998) Discrepancies between the NMR and X-ray structures of uncomplexed barstar: analysis suggests that packing densities of protein structures determined by NMR are unreliable, *Biochemistry 37*, 6958−6966.
2. Lubienski, M. J., Bycroft, M., Freund, S. M., and Fersht, A. R. (1994) Three-dimensional solution structure and ^{13}C assignments of barstar using nuclear magnetic resonance spectroscopy, *Biochemistry 33*, 8866−8877.
3. Wong, K. B., Fersht, A. R., and Freund, S. M. (1997) NMR ^{15}N relaxation and structural studies reveal slow conformational exchange in barstar C40/82A, *J. Mol. Biol. 268*, 494−511.
4. Korchuganov, D. S., Nolde, S. B., Reibarkh, M. Y., Orekhov, V. Y., Schulga, A. A., Ermolyuk, Y. S., Kirpichnikov, M. P., and Arseniev, A. S. (2001) NMR study of monomer-dimer equilibrium of barstar in solution, *J. Am. Chem. Soc. 123*, 2068−2069.
5. Martinez, J. C., Filimonov, V. V., Mateo, P. L., Schreiber, G., and Fersht, A. R. (1995) A calorimetric study of the thermal stability of barstar and its interaction with barnase, *Biochemistry 34*, 5224−5233.
6. Schreiber, G., and Fersht, A. R. (1993) The refolding of cis- and trans-peptidylprolyl isomers of barstar, *Biochemistry 32*, 11195−11203.
7. Wintrode, P. L., Griko, Y. V., and Privalov, P. L. (1995) Structural energetics of barstar studied by differential scanning microcalorimetry, *Protein Sci. 4*, 1528−1534.
8. Golbik, R., Fischer, G., and Fersht, A. R. (1999) Folding of barstar C40A/C82A/P27A and catalysis of the peptidyl-prolyl cis/trans isomerization by human cytosolic cyclophilin (Cyp18), *Protein Sci. 8*, 1505−1514.
9. Killick, T. R., Freund, S. M., and Fersht, A. R. (1999) Real-time NMR studies on a transient folding intermediate of barstar, *Protein Sci. 8*, 1286−1291.
10. Nolting, B., Golbik, R., and Fersht, A. R. (1995) Submillisecond events in protein folding, *Proc. Natl. Acad. Sci. U.S.A. 92*, 10668−10672.
11. Nolting, B., Golbik, R., Neira, J. L., Soler-Gonzalez, A. S., Schreiber, G., and Fersht, A. R. (1997) The folding pathway of a protein at high resolution from microseconds to seconds, *Proc. Natl. Acad. Sci. U.S.A. 94*, 826−830.
12. Lee, L. P., and Tidor, B. (2001) Barstar is electrostatically optimized for tight binding to barnase, *Nat. Struct. Biol. 8*, 73−76.
13. Vaughan, C. K., Buckle, A. M., and Fersht, A. R. (1999) Structural response to mutation at a protein-protein interface, *J. Mol. Biol. 286*, 1487−1506.
14. Labroo, V. M., Hebel, D., Kirk, K. L., Cohen, L. A., Lemieux, C., and Schiller, P. W. (1991) Direct electrophilic fluorination of tyrosine in dermorphin analogues and its effect on biological activity, receptor affinity and selectivity, *Int. J. Pept. Protein Res. 37*, 430−439.
15. Li, H., and Frieden, C. (2006) Fluorine-19 NMR studies on the acid state of the intestinal fatty acid binding protein, *Biochemistry 45*, 6272−6278.
16. Eletsky, A., Atreya, H. S., Liu, G., and Szyperski, T. (2005) Probing structure and functional dynamics of (large) proteins with aromatic rings: L-GFT-TROSY (4,3)D HCCH NMR spectroscopy, *J. Am. Chem. Soc. 127*, 14578−14579.
17. Wuthrich, K., Wagner, G., Richarz, R., and Braun, W. (1980) Correlations between internal mobility and stability of globular proteins, *Biophys. J. 32*, 549−560.

18. Wagner, G., DeMarco, A., and Wuthrich, K. (1976) Dynamics of the aromatic amino acid residues in the globular conformation of the basic pancreatic trypsin inhibitor (BPTI). I. ^{1}H NMR studies, *Biophys. Struct. Mech. 2*, 139−158.
19. Wagner, G. (1983) Characterization of the distribution of internal motions in the basic pancreatic trypsin inhibitor using a large number of internal NMR probes, *Q. Rev. Biophys. 16*, 1−57.
20. Wagner, G., Bruhwiler, D., and Wuthrich, K. (1987) Reinvestigation of the aromatic side-chains in the basic pancreatic trypsin inhibitor by heteronuclear two-dimensional nuclear magnetic resonance, *J. Mol. Biol. 196*, 227−231.
21. Skalicky, J. J., Mills, J. L., Sharma, S., and Szyperski, T. (2001) Aromatic ring-flipping in supercooled water: implications for NMR-based structural biology of proteins, *J. Am. Chem. Soc. 123*, 388−397.
22. Campbell, I. D., Dobson, C. M., Moore, G. R., Perkins, S. J., and Williams, R. J. (1976) Temperature dependent molecular motion of a tyrosine residue of ferrocytochrome C, *FEBS Lett. 70*, 96−100.
23. Nall, B. T., and Zuniga, E. H. (1990) Rates and energetics of tyrosine ring flips in yeast iso-2-cytochrome *c*, *Biochemistry 29*, 7576−7584.
24. Li, H., and Frieden, C. (2005) NMR studies of 4-^{19}F-phenylalanine-labeled intestinal fatty acid binding protein: evidence for conformational heterogeneity in the native state, *Biochemistry 44*, 2369−2377.
25. Rami, B. R., Krishnamoorthy, G., and Udgaonkar, J. B. (2003) Dynamics of the core tryptophan during the formation of a productive molten globule intermediate of barstar, *Biochemistry 42*, 7986−8000.
26. Shastry, M. C., and Udgaonkar, J. B. (1995) The folding mechanism of barstar: evidence for multiple pathways and multiple intermediates, *J. Mol. Biol. 247*, 1013−1027.
27. Zaidi, F. N., Nath, U., and Udgaonkar, J. B. (1997) Multiple intermediates and transition states during protein unfolding, *Nat. Struct. Biol. 4*, 1016−1024.
28. Pradeep, L., and Udgaonkar, J. B. (2002) Differential salt-induced stabilization of structure in the initial folding intermediate ensemble of barstar, *J. Mol. Biol. 324*, 331−347.
29. Pradeep, L., and Udgaonkar, J. B. (2004) Osmolytes induce structure in an early intermediate on the folding pathway of barstar, *J. Biol. Chem. 279*, 40303−40313.
30. Rami, B. R., and Udgaonkar, J. B. (2002) Mechanism of formation of a productive molten globule form of barstar, *Biochemistry 41*, 1710−1716.
31. Sridevi, K., Lakshmikanth, G. S., Krishnamoorthy, G., and Udgaonkar, J. B. (2004) Increasing stability reduces conformational heterogeneity in a protein folding intermediate ensemble, *J. Mol. Biol. 337*, 699−711.
32. Pace, C. N., and Schmid, F. X. (1997) *Protein structure: A practical approach*, pp 253−260.
33. Frieden, C., Hoeltzli, S. D., and Bann, J. G. (2004) The preparation of ^{19}F-labeled proteins for NMR studies, *Methods Enzymol. 380*, 400−415.
34. Ropson, I. J., Gordon, J. I., and Frieden, C. (1990) Folding of a predominantly beta-structure protein: rat intestinal fatty acid binding protein, *Biochemistry 29*, 9591−9599.
35. Santoro, M. M., and Bolen, D. W. (1988) Unfolding free energy changes determined by the linear extrapolation method. 1. Unfolding of phenylmethanesulfonyl alpha-chymotrypsin using different denaturants, *Biochemistry 27*, 8063−8068.
36. Delaglio, F., Grzesiek, S., Vuister, G. W., Zhu, G., Pfeifer, J., and Bax, A. (1995) NMRPipe: a multidimensional spectral processing system based on UNIX pipes, *J. Biomol. NMR 6*, 277−293.
37. Bain, A. D., Rex, D. M., and Smith, R. N. (2001) Fitting dynamic NMR lineshapes, *Magn. Reson. Chem. 39*, 122−126.
38. Eyring, H. J. (1935) The activated complex in chemical reactions, *J. Chem. Phys. 3*, 107−115.
39. Wong, K. B., Freund, S. M., and Fersht, A. R. (1996) Cold denaturation of barstar: ^{1}H, ^{15}N and ^{13}C NMR assignment and characterisation of residual structure, *J. Mol. Biol. 259*, 805−818.
40. Swaminathan, R., Nath, U., Udgaonkar, J. B., Periasamy, N., and Krishnamoorthy, G. (1996) Motional dynamics of a buried tryptophan reveals the presence of partially structured forms during denaturation of barstar, *Biochemistry 35*, 9150−9157.
41. Wong, K. B., and Daggett, V. (1998) Barstar has a highly dynamic hydrophobic core: evidence from molecular dynamics simulations and nuclear magnetic resonance relaxation data, *Biochemistry 37*, 11182−11192.
42. Li, H., and Frieden, C. (2005) Phenylalanine side chain behavior of the intestinal fatty acid binding protein: The effect of urea on backbone and side chain stability, *J. Biol. Chem. 280*, 38556−38561.
43. Hodsdon, M. E., and Frieden, C. (2001) Intestinal fatty acid binding protein: the folding mechanism as determined by NMR studies, *Biochemistry 40*, 732−742.
44. Bhavesh, N. S., Juneja, J., Udgaonkar, J. B., and Hosur, R. V. (2004) Native and nonnative conformational preferences in the urea-unfolded state of barstar, *Protein Sci. 13*, 3085−3091.
45. Privalov, P. L. (1990) Cold denaturation of proteins, *Crit. Rev. Biochem. Mol. Biol. 25*, 281−305.
46. Whitten, S. T., Kurtz, A. J., Pometun, M. S., Wand, A. J., and Hilser, V. J. (2006) Revealing the nature of the native state ensemble through cold denaturation, *Biochemistry 45*, 10163−10174.
47. Pometun, M. S., Peterson, R. W., Babu, C. R., and Wand, A. J. (2006) Cold denaturation of encapsulated ubiquitin, *J. Am. Chem. Soc. 128*, 10652−10653.
48. Sadqi, M., Fushman, D., and Munoz, V. (2006) Atom-by-atom analysis of global downhill protein folding, *Nature 442*, 317−321.
49. Lakshmikanth, G. S., Sridevi, K., Krishnamoorthy, G., and Udgaonkar, J. B. (2001) Structure is lost incrementally during the unfolding of barstar, *Nat. Struct. Biol. 8*, 799−804.
50. Koradi, R., Billeter, M., and Wuthrich, K. (1996) MOLMOL: a program for display and analysis of macromolecular structures, *J. Mol. Graphics 14*, 51−55, 29−32.

BI6026083